

Synthesis and Characterization of Heterogeneous Catalysts and Comparison to Iron-ore

Khelifi S*, Ayari F, Hassan Chehimi DB and Trabelsi-Ayadi M

Laboratory of Applications of Chemistry to Resources and Natural Substances and to the Environment (LACReSNE), Faculty of Sciences of Bizerte, University of Carthage, Zarzouna 7021, Tunisia

Abstract

The placement of metal oxide pillars between clay mineral layers modifies their physicochemical properties, including surface area, acidity, and catalytic activity. Aluminum is the most commonly used pillar cation, but the use of Fe offers a distinct opportunity to expand the range of catalytic behavior. The purpose of this study was to prepare Al-Fe-pillared smectite and to characterize the resulting materials. Al-Fe-pillared clay was synthesized from Tunisian clay precursors according to a common procedure: grinding, sieving, Na exchange, pillaring, drying and calcinations. Smectite suspension was mixed with different pillaring solutions containing Al and Fe oligomers with Fe/(Al+Fe) percent ratios: 1; 5; 10 and 50%. Other types of material were investigated in this work; natural iron-ore was defined and characterized as heterogeneous catalysis. The structural and textural properties of synthesis and natural catalysis have been determined by X-ray diffraction, nitrogen adsorption-desorption isotherms, Transmission Electron Microscopy (MET), X-ray fluorescence, CEC and infrared spectroscopy.

Keywords: Clay; Al-Fe pillared clays; Catalysts; Iron-ores

Introduction

Wastewaters have become a major social and economic problem as modern health-quality standards and environmental regulations are gradually being more restrictive [1]. Among these pollutants an increased concern is directed towards organic refractory compounds which are difficult to remove by means of conventional wastewater treatment technologies. One of the most promising solutions for the elimination of pollutants from waste waters is catalytic wet peroxide oxidation (CWPO) using pillared clays, will probably constitute the best option in the near future. It has been proven as a method extremely effective under mild conditions for the degradation of almost all organic compounds to CO₂, H₂O and inorganic ions [2]. Pillaring is a process of smectite modification used to obtain materials that have found a wide range of applications in catalytic, adsorption and separation processes [3-5]. Common procedure for pillared clay (PILC) preparation is: swelling of smectite in water, exchange of the interlayer cations by partially hydrated polymeric or oligomeric metal cation complexes in the interlamellar region of the starting clay, drying and calcining of wet cake formed of expanded clay to have the metal polyoxocations transformed into metal oxide pillars [6].

Very often, the introduction of a catalyst will improve the process performances as the reaction rates increase through a better elimination of the pollutants and more selective usage of the oxidizing agent [6]. As a result, the technology costs are also lowered. As far as soluble catalysts might hardly be separated from the treated effluents, most researches concentrated on the development of stable heterogeneous catalysts for the complete mineralization of the organic pollutants. Heterogeneous catalysis has several advantages over homogeneous catalysis: (1) simplicity in synthetic operations; (2) prevention of the production of salt wastes during neutralisation of the catalysts or reagents; and (3) reusability of the solid catalyst [7-10].

Pillared clays are very interesting and promising catalysts with a broad range of applications, such as acid-catalyzed reactions and synthesis, since the pillared clays present higher surface areas, microporosity and thermal stability than those of the parent clays. Al-Fe PILCs have been reported as active catalysts in oxidation reactions of environmental interest [11-16]. The iron (III) species incorporated

into the pillars between the clay layers are the active sites for the oxidation reaction [17]; meanwhile, the Al polyhydroxocations are needed for facilitating the pillaring of the solid and increasing its microporosity [18].

Different solids have been employed to catalyze the oxidation of organic compounds in wastewaters: transition-metal oxides and noble metals have been extensively used as active components. Transition metal exchanged zeolites [19,20] and Cu⁺² or Fe⁺³-montmorillonites have been proposed as active catalysts for organic compounds oxidation in aqueous phase [21-24]. On the other hand iron is the metallic ion used in Fenton's reagent [25], thus, the intercalation of cations Al-Fe in the interlayer spacing of smectite should produce catalytically active materials for oxidation of organic compounds with hydrogen peroxide. Pillared clays have received increasing interest in the last 2 decades due to their textural and catalytic properties in different reactions. They represent a new class of microporous materials that have potential applications as catalysts [26]. PILC properties are affected by various synthesis parameters such as solid/liquid ratio, clay origin, particle size, type of oligomeric metal cation or mixture of cations, intercalation conditions, temperature and duration of calcining. In this work the pillaring process was performed on one fraction of Tunisian-originated clay. PILC catalysts based on smectite-Na with Al³⁺ and Fe³⁺ as active cations were synthesized where several synthesis parameters were maintained constant such as clay size and origin, type of pillaring cations and their ratio, cation/clay ratio. On the other hand, four extreme pillaring cations ratio sets of parameters were applied and their

*Corresponding author: Selma Khelifi, Laboratory of Applications of Chemistry to Resources and Natural Substances and to the Environment (LACReSNE), University of Carthage, Faculty of Sciences of Bizerte, Zarzouna 7021, Tunisia, Tel: +21653111929; E-mail: Selma.khelifi@gmail.com

Received November 18, 2016; Accepted November 30, 2016; Published December 04, 2016

Citation: Khelifi S, Ayari F, Hassan Chehimi DB, Trabelsi-Ayadi M (2016) Synthesis and Characterization of Heterogeneous Catalysts and Comparison to Iron-ore. J Chem Eng Process Technol 7: 316. doi: 10.4172/2157-7048.1000316

Copyright: © 2016 Khelifi S, et al. This is an open-access article distributed under the terms of the Creative Commons Attribution License, which permits unrestricted use, distribution, and reproduction in any medium, provided the original author and source are credited.

influence on the catalyst properties was investigated. In the other hand, utilization of natural heterogeneous catalyst in Fenton process could be a potential alternative owing to their low cost and abundance. So, a natural iron-ore was defined and characterized in this study.

Experimental Section

Starting materials

The raw clay: The starting material was a smectite extracted from soils of Teboursouk (North-West of Tunisia). This clay underwent a purification stage per the procedure given in this work [27] before synthesis of Fe-Al intercalated montmorillonites as follows: 100 g of raw clay (particle size <100 μm) was added into 1 L of Na_2CO_3 solution (1 $\text{mol}\cdot\text{L}^{-1}$) and stirred at 80°C for 3 h. During the stirring, several drops of HCl were added into the suspension to dissolve the CO_3^{2-} . Na-smectite was collected by centrifugation and washed with deionized water until the solution was free of chloride (titration with AgNO_3) [28]. The Na-smectite was dried at 80°C , ground through a 60-mesh sieve and kept in a sealed bottle. The surface area and CEC were $592.70\text{ m}^2/\text{g}$ and $72.93\text{ meq}/100\text{ g}$. The chemical composition and the X-ray diffraction pattern are reported in Figure 1. The structural formula is $\text{Ca}_{0.33}\text{Na}_{0.02}\text{K}_{0.05}(\text{Si}_{6.84}\text{Al}_{1.16})(\text{Al}_{2.55}\text{Fe}_{1.12}\text{Mg}_{0.72})\text{O}_{22}$. All solutions and dispersions were prepared using deionized water. $\text{AlCl}_3\cdot 6\text{H}_2\text{O}$, $\text{FeCl}_3\cdot 6\text{H}_2\text{O}$, Na_2CO_3 and NaOH were purchased from Sigma-Aldrich.

Natural iron-ore: Two samples were collected by works staff from iron-ore career situated at Tamra region in the north-West of Tunisia. Samples were dried after collection and crushed twice to reduce particle size. Natural catalyst being labeled MF and MF01.

Synthesis of pillared clay

Preparation of the pillaring agents: Al-Fe-pillared clays (Al-Fe-PILCs) were synthesized by the reaction of Na-smectite with base-hydrolyzed solutions of Fe and Al. The process of pillaring was carried out according to a common procedure [29,30] with simple modification. The Fe/(Fe+Al) ratios (Fe: Fe^{3+} and Al: Al^{3+}) used were 0.01; 0.05; 0.10 and 0.50. An intercalant solution was prepared by titration of an $\text{Al}^{3+}/\text{Fe}^{3+}$ cationic solution with 0.2M NaOH. The cationic solution consisted of 0.18M $\text{AlCl}_3\cdot 6\text{H}_2\text{O}$ and 0.02M $\text{FeCl}_3\cdot 6\text{H}_2\text{O}$. The addition of the NaOH solution to the cationic solution was attempted under stirring at a controlled rate and at 70°C for 12 hours while the amount of the NaOH solution added was such that the final OH/cation ratio was equal to 1.9. These pillaring solutions which give Fe-polyhydroxy and Al-polyhydroxy species were aged for 7 days out at room temperature before use. A nomenclature was used for the PILCs where the first

letters, Al or Fe, respectively indicated the absence or presence of iron in the pillaring solutions, and the following numbers indicated the used Fe/(Al+Fe) ratio: Fe-0.01-PILC, Fe-0.05-PILC, Fe-0.1-PILC and Fe-0.5-PILC.

Pillaring process: The PILCs were prepared by adding dropwise the pillaring solution to a 2% suspension of homoionic smectite under stirring to give a metal/ clay ratio of $3.8\text{ mMol}\cdot\text{g}^{-1}$. The suspension was aged for 1 day at room temperature. Then, the resulting dispersion was left for 24 h and the excess supernatant was removed. The sediment was dialyzed with distilled water until chloride was absent [28]. Finally, the pillared clay precursor was dried at $60\text{--}70^\circ\text{C}$ and their calcinations were happened at 500°C for 2 h. Dehydration and dehydroxylation occur upon calcination to give metal oxide clusters which act as pillars. Four solids were prepared: Fe-0.01-PILC, Fe-0.05-PILC, Fe-0.1-PILC and Fe-0.5-PILC.

Characterization methods: The catalysts were characterized using several techniques to identify the structural and physicochemical properties. The chemical composition of the PILC was determined by X-ray fluorescence. All XRF measurements were performed with a commercial instrument (ARL 9900 of THERMOFISHER), using monochromatic radiation $K_{\alpha 1}$ of cobalt ($\lambda=1.788996\text{ \AA}$). The crystalline form of the catalyst was identified by X-ray diffractometer (XRD) using a PANalytical X'Pert HighScore Plus diffractometer, $\text{CuK}\alpha$ radiation. X-ray diffraction spectra were recorded on samples dried at room temperature for all catalysts and after calcinations for 2 h at 300°C , 500°C and 750°C for pillared clays. Oriented films were prepared on glass slides. The data were collected from 2° to $60^\circ 2\theta$. These data allowed the calculation of the d_{001} spacing which was shown to be characteristic of the interlamellar spacing for pillared clays. The textural parameters of the samples were studied by means of the adsorption-desorption isotherms of N_2 at 77K using a Quantachrome model Nova 1200e surface and porosity analyser. Prior to the measurement, samples were outgassed at a temperature of 200°C under high vacuum for 2 h. Specific BET surface area (S_{BET}) values were calculated with $0.05 < P/P_0 < 0.30$. The total pore volume (V_t) was estimated from the adsorption data at a P/P_0 value of ~ 0.99 . The Barrett-Joyner-Halenda (BJH) method was applied to the desorption data for P/P_0 values above 0.20 to determine the mesopore surface area (S_{BJH}) and the mesopore volume (V_{BJH}) for pores in the $10\text{--}500\text{ \AA}^3$ range. The mesopore volume distribution as a function of pore size was calculated by (BJH) method. Cation Exchange Capacity (CEC) were determined by the copper ethylenediamine complex $\text{Cu}(\text{EDA})_2^{2+}$ method [31,32].

Fourier transform infrared (FT-IR) analysis was done to identify the functional groups associated with the catalyst. FT-IR spectra were collected on a Perkin Elmer 783 dispersive spectrometer in the range of $4000\text{--}400\text{ cm}^{-1}$.

The morphology of natural clay and the catalyst was studied using TEM. Elemental composition was identified by EDX energy dispersive X-ray microanalysis. Samples for TEM analysis were prepared by dispersing the powdered sample in ethanol by sonication and then drop drying on a copper grid (400 mesh) coated with carbon film.

Results and Discussion

Pillared clay characterization

The Table 1 shows the clay mineral elemental composition obtained from the raw clay and after pillaring with Al-Fe oligomers. Intercalation of these oligomers was successful as noted in the increase in Al and Fe content relative to the initial clay mineral in concordance with Fe/

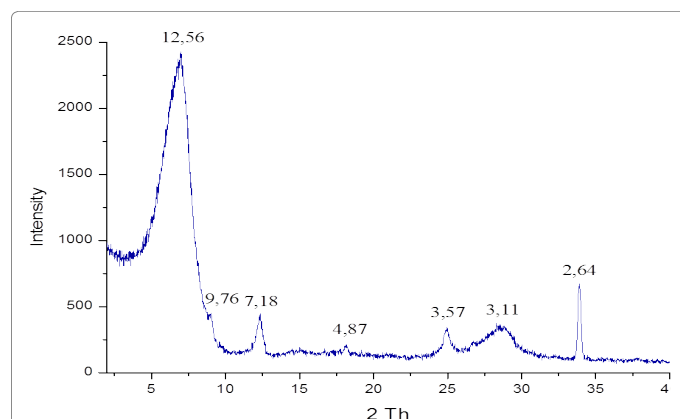


Figure 1: X-ray diffraction pattern and chemical composition of the natural clay.

(Al+Fe) ratio used in the pillaring process. However, a decrease in Al content was observed in Fe-0.5-PILC which contains the highest amount of Fe. This could be a consequence of aluminum dissolution or also due to isomorphous substitution of aluminum by iron on the octahedral network [33]. There is also a decrease in the octahedral Mg content in the pillared clay minerals due to the attack of protons from the oligomeric cations, which are decomposed after heating in oxide pillars with the subsequent proton release [34]. This Mg release yielded hydroxyl acid sites.

X-ray diffraction

The X-ray diffractograms corresponding to the PILC by intercalation of Al and Fe oligomers are shown in Figure 2. The XRD results indicate that the modification carried out over the clay leads, in all the cases, to the successful pillaring of the material, revealing the shift of the signal d_{001} to higher values between 19 Å and 14 Å. This peak was broadened and its intensity weakened by the incorporation of Fe-Al complexes, indicating that the Fe-Al complexes were intercalated randomly into the interlayer of smectite [35]. The d_{001} values were clearly much greater at a relatively small Fe/(Al+Fe) ratio, while they decreased to 14.49 Å at Fe/(Al+Fe)=0.5, similar to previous results in which an increase of the Fe content produced materials with little increase in the basal spacing [36-39]. In the other hand, some research was done at low angle $2\theta=1^\circ$ which showed an additional peak at 52 Å [40], 72 Å [41], 76 Å [42]. This peak at low angle was of lower intensity compared to that at 18 Å. These studies explained the d_{001} values obtained in the current study especially for an Fe/(Al+Fe) ratio of 0.5 who is almost similar of previous studies performed with Fe-Al based PILCs with starting angle

$2\theta=2^\circ$ [13,14,43-45] which showed the largest basal spacing of about 25 Å, 19 Å, 17 Å. The simple different observed can be due to the different (Fe+Al)/OH ratios used in the formation of the Fe and Al oligomers, since the pillaring process is strongly dependent on experimental conditions such as temperature, pH and dependent on the nature of the exchangeable cation and especially on the metal/base ratio used.

For more explanation of this phenomena, catalysis based Fe-PILC was synthesized with Fe/(Fe+Al) ratio equal to 1. The XRD patterns of this sample and the raw clay are presented in Figure 3. The great reflection observed in $2\theta=2.3^\circ$ is related to basal spacing d_{001} (37.41 Å) confirming the success of the pillaring process. The second reflection at $2\theta=6.04^\circ$ relative to 14.65 Å. Other diffractions are related to the presence of iron oxide: hematite ($2\theta=33.3^\circ$; 40.53° ; 49.10° ; 67.56°) and magnetite ($2\theta=35.18^\circ$; 53.69° ; 63.62°). These results indicate that iron not only entered the clay layers, but also a portion of it was deposited out of the layer. But, there is no diffraction of iron or aluminum oxide in the patterns of all Al-Fe-PILCs samples, suggesting that Al species are totally inserted on the clay or that the iron and aluminum oxides particles are very small particles.

Furthermore, pillared clays have been calcined at some temperature for investigate the temperature effect. The obtained results are figured in Figure 4 at four temperatures: at room temperature, 300°C, 500°C and 650°C. The d_{001} values does not undergo a large variation. So, these results improve the thermal stability of materials synthesized.

Textural properties

The Figure 5 shows the N_2 isotherms at 77 K for natural clay and Fe-Al-PILCs samples. The isotherms are of type IV, corresponding to microporous solids and parallel from $P/P_0 > 0.2$. This indicates that the nitrogen adsorbed from this point to $P/P_0 = 0.98$ was similar in all types of samples. The presence of micropores is generated in the pillaring process to intercalate inorganic polyoxycations between the clay layers. All samples show a hysteresis loop type H_4 according to IUPAC classification.

The Table 2 presents the values for specific surface area, S_{BET} , volume of N_2 adsorbed at $P/P_0 = 0.98$; V_{ads} , mesoporosity surface and volume; $S_{BJH/msp}$ and $V_{BJH/msp}$ respectively, from the Barret-Joyner-Halenda method [46] and average pore diameter (D) of the different samples.

It's seen that all pillared clays have similar textural properties and

% oxides	Cp	Fe-0.01-PILC	Fe-0.05-PILC	Fe-0.1-PILC	Fe-0.5-PILC
SiO ₂	55.21	53.08	52.14	52.00	53.34
Al ₂ O ₃	20.09	27.32	28.23	28.87	20.14
Fe ₂ O ₃	7.10	9.36	10.68	12.19	18.28
K ₂ O	0.29	1.21	1.16	1.02	1.10
MgO	3.33	2.94	2.93	2.84	2.44
Na ₂ O	1.97	0.23	0.21	0.18	0.19
CaO	0.13	0.088	0.09	0.097	0.10
SO ₃	0.81	0.81	0.80	0.83	0.79
P ₂ O ₅	0.10	0.10	0.09	0.06	0.09
LOI	11.27	6.27	6.18	4.05	4.64

LOI: loss on ignition

Table 1: Chemical analysis of the raw clay mineral and PILCs expressed as oxide percentage.

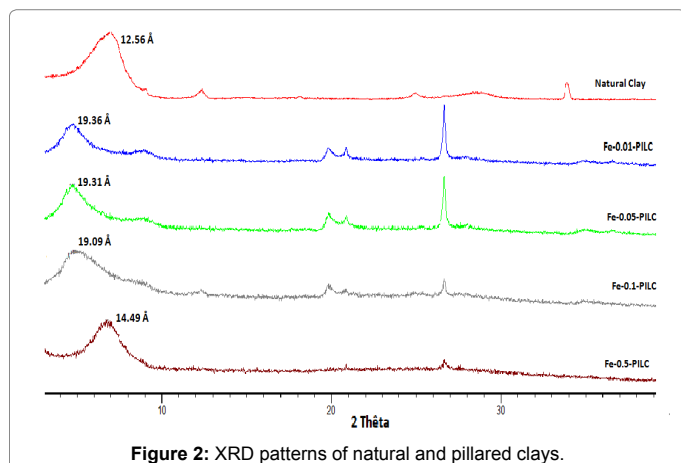


Figure 2: XRD patterns of natural and pillared clays.

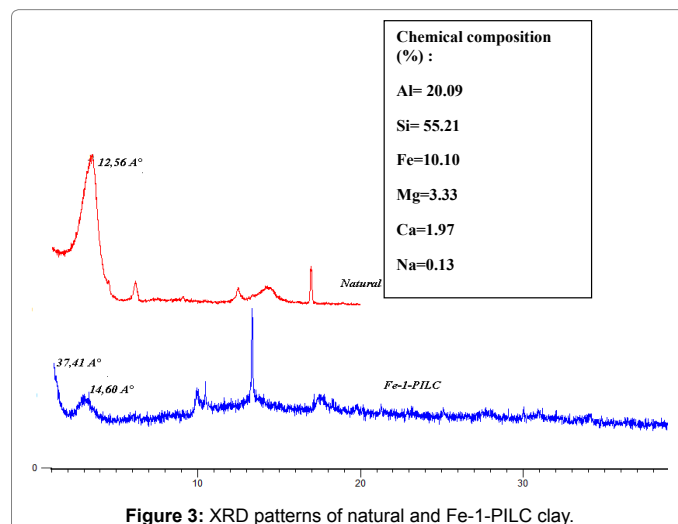


Figure 3: XRD patterns of natural and Fe-1-PILC clay.

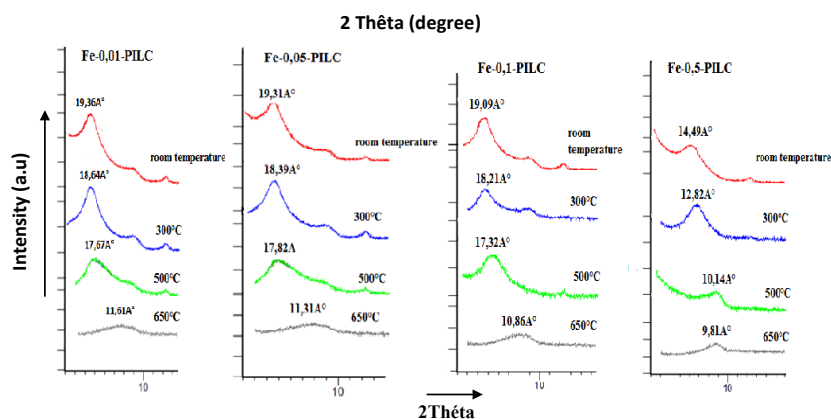


Figure 4: X-ray diffraction patterns of the calcined Al-Fe-PILCs at 300°C, 500°C and 650°C.

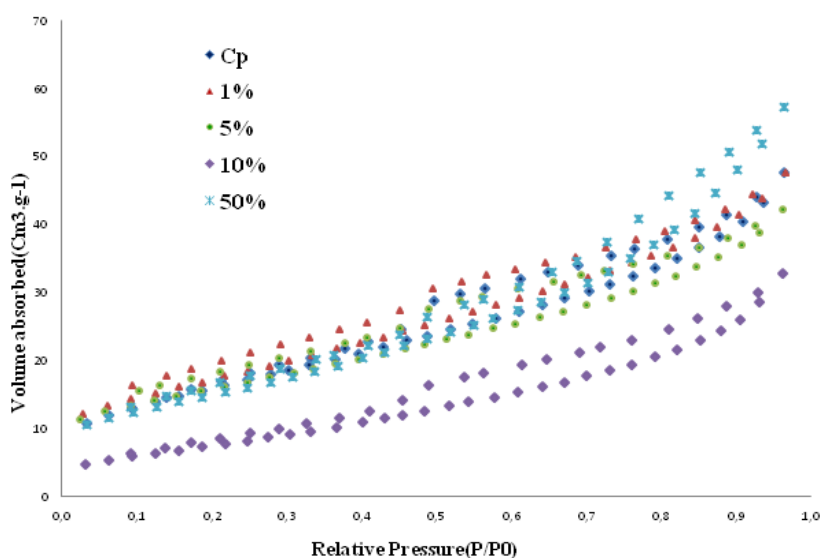


Figure 5: Adsorption-desorption isotherms of the PILCs and natural clay.

Samples	S_{BET} (m ² /g)	$S_{BJH/mesp}$ (m ² /g)	V_{ads} (cm ³ /g)	$V_{BJH/mesp}$ (cm ³ /g)	D(A°)
Natural clay	57.963	38.316	0.07	0.059	19.109
Fe-0.01-PILC	61.673	34.706	0.08	0.063	18.848
Fe-0.05-PILC	55.429	30.856	0.07	0.046	18.904
Fe-0.1-PILC	50.086	30.069	0.05	0.047	19.003
Fe-0.5-PILC	53.854	44.278	0.09	0.078	18.848

S_{BET} : BET surface area, $S_{mesp/BJH}$: mesopore surface area, $V_{mesp/BJH}$: mesopore volume, V_{ads} : volume of N₂ adsorbed at P/P₀ = 0.98, D: average pore diameter.

Table 2: Textural parameters of the samples: Natural and pillared clay.

these properties do not change remarkably with different synthesis conditions. The similar textural properties of these samples may be explained by the formation of a similar sized basal spacing and similar dispersions of the pillars in the interlayer region. However, synthesized catalysts have a greater d_{001} value than the parental clay, but they have a lower S_{BET} value, which is associated with the amount and dispersion of the pillars among the interlayer of these samples. Furthermore, BET surface area of the parental clays decreases after the intercalation with Fe and Al polycations, possibly due to the formation of iron oxide nanoparticles covering the external surface and clogging the micropore of the clay support. However, the micropore area decreased from Fe-0.01-PILC to

Fe-0.5-PILC. The larger decrease for the micropore area vs. the total surface area indicated that most of the new surface area created in the pillaring process with Fe species corresponded to mesopores. Also, a uniform pore size and volume pore is observed for all the catalysts (Figure 6). This result is similar to that for the parental clay. The BJH-mesopore size distributions obtained from the nitrogen adsorption isotherms for the samples that were studied are presented in Figure, as can be seen from Figure, there is a good agreement between the pore size distributions of the samples studied.

The Table 2 reports the basal spacing (d_{001}) after calcinations at different temperature, BET surface area of pillared clays. The corresponding values of the starting smectite calcinated at the same temperatures are also included for comparison. As can be seen, the basal spacing decreases when the calcinations temperature is increased owing to the dehydroxylation of the pillars. The pillaring process substantially increases the basal spacing and decrease BET surface area. Indeed, these pillars separate adjacent silicate layers which then increases the interlayer distance and creates a permanent porosity between them.

Transmission electron microscopy-EDX

The morphological changes of the solid particles were observed

by Transmission Electron Microscopy (TEM). Figure 7 depicts TEM micrographs of the natural and pillared clay. In this paper, we give only the example of Fe-0.1-PILC. For viewing the clay particles mainly parallel to the c-axis, a dilute suspension of material in 70% alcohol was briefly ultrasonicated and a small drop of the suspension was placed on a thin carbon film on a TEM copper grid, allowed to dry and coated

with a thin carbon layer to improve stability under the beam. It can be learned that Na-smectite has a layered structure and a two-dimension porous structure with small basal spacing. For Fe-0.1-PILC the layers were obviously kept apart, obtaining large pore structures, and the basal spacing between two neighboring fringes was discarded, corresponding to the successful pillaring (Figure 7c and 7f).

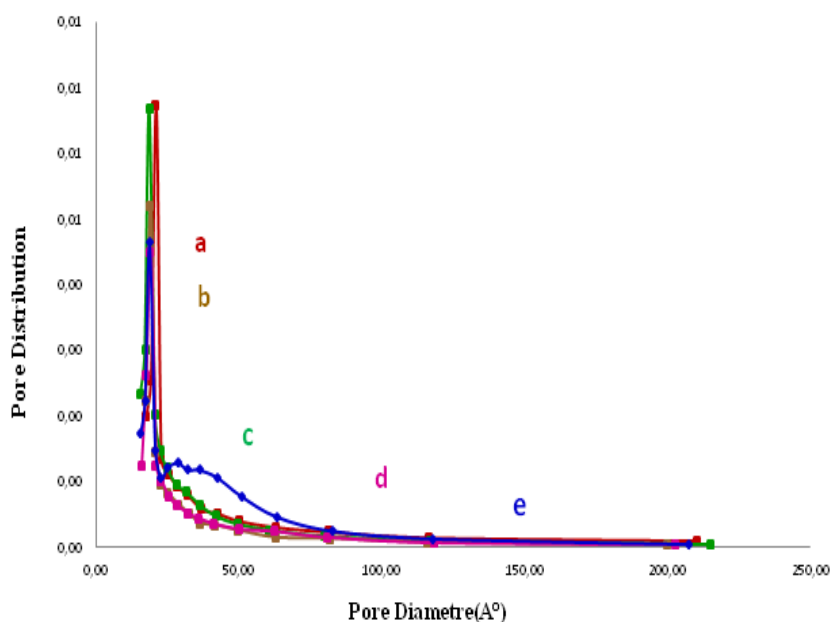


Figure 6: BJH-method pore size distribution curves from nitrogen sorption data. a=natural, b=1%, c=5%, d=10%, e=50%.

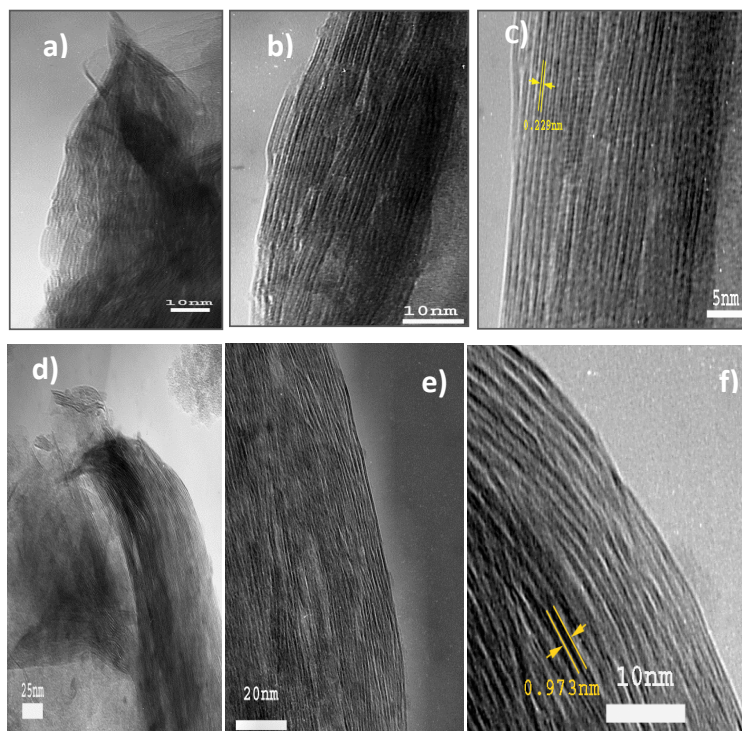


Figure 7: Morphology of natural clay and Fe-0.1-PILC at different scale: Natural clay: 10 nm (a) (b) and 5 nm (d) Fe-0.1-PILC: 25 nm (d), 20 nm (e) and 10 nm (f) given by TEM.

The EDX analysis is consistent with the expected presence of Fe and Al in Fe-0.1-PILC. This confirms the reality insertion of the raw material. Figure 8 presents the spectrum of Fe-0.1-PILC and natural clay.

IR spectroscopy

The Figure 9 illustrates the FTIR analysis of the natural clay and all the Al-Fe-PILCs. The spectra of Al-Fe-pillared clays show that several bands typical of smectite (3624 cm^{-1} for O-H stretching of structural O-H groups, 1087 cm^{-1} for Si-O stretching, 914 cm^{-1} of Al-Al-OH deformation, 795 cm^{-1} for Si-O stretching of cristobalite, 626 cm^{-1} for coupled Al-O and Si-O out of plane stretching vibration, 519 cm^{-1} Al-O-Si deformation, and 467 cm^{-1} of Si-O-Si deformation) are nearly the same or the change in these bands is insignificant after pillaring. Major change was observed in three areas of wavelength range, at 3430 cm^{-1} , 1640 cm^{-1} , and 797 cm^{-1} . The absorption at 3430 cm^{-1} can be assigned to the symmetric O-H stretching vibration of H-bonded water [47]; the frequency shifted to a higher, then back to a lower, wavenumber with increasing Fe/Al+Fe molar ratio. Comparison between intercalated samples revealed that Fe contributed to the decrease of hydrogen-bonding strength in Al-Fe-PILC. Meanwhile, the H-O-H bending vibration at 1642 cm^{-1} found in smectite shifted to 1634 cm^{-1} after intercalation.

Cation Exchange Capacity: CEC

The CEC value of pillared clays samples shows a decrease with the amount of added Fe/(Fe+Al) (from 24 to 13 méq/100 g) indicating

that the exchangeable cations and the protons were replaced by pillars incorporated into the clay. The Table 3 shows these experiments results.

Iron-ores characterization

The component analyses of the studied iron-ore were shown in Table 4. As evident from the results in the table, that Fe, Si and Ca are the three most abundant elements in the samples, the Fe grades of all samples were higher than 50%, the sample MF01 contains the highest amount of iron and the ignition loss (LOI) values varied from 9-11.2%. The Alumina (Al_2O_3) content normally ascribed to kaolinite varied from 3.9 to 5.03%. The silica (SiO_2) grades were much higher than 10%. Also worth noting is these iron ore all contain some toxic heavy metals.

Textural characterization

BET analysis was used to investigate the microstructural properties of natural iron-ore samples. BET surface area analyses (Table 5) indicate the studied samples have similar S_{BET} , 44.3 and $45.86\text{ m}^2/\text{g}$ for MF and MF01 respectively. A uniform pore size and volume pore is observed for both catalysts (Table 5). The adsorption-desorption isotherms of all samples are a type IV isotherm with a hysteresis loop according to IUPAC classification [48]. As shown in Figure 10 the most probable values of samples pore size are about 2 nm indicating they are microporous materials.

Mineralogical characterization

The XRD analysis was applied to define the structure of both iron-

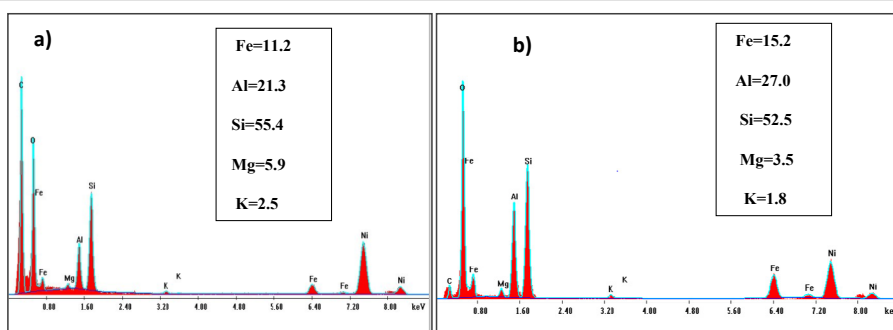


Figure 8: EDAX spectrum of natural clay (a) and Fe-0.1-PILC (b).

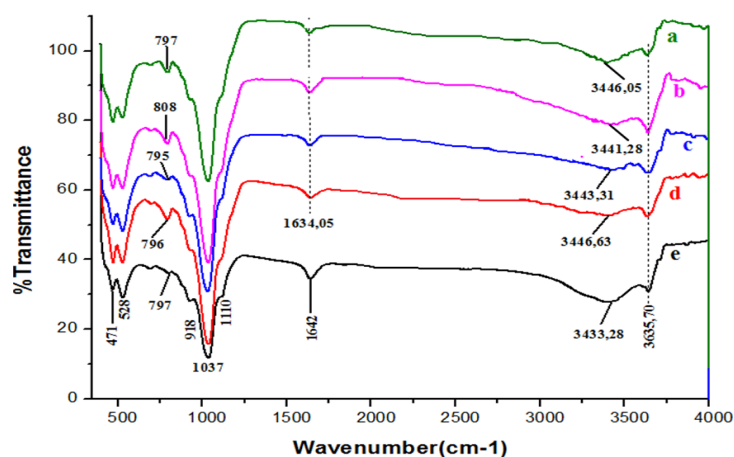


Figure 9: Infrared spectra of natural (e) and pillared clays: (a) Fe-0.5-PILC; (b) Fe-0.1-PILC; (c) Fe-0.05-PILC and (d) Fe-0.01-PILC.

Solids	Natural clay	Al-Fe-0.01-PILC	Al-Fe-0.05-PILC	Al-Fe-0.1-PILC	Al-Fe-0.5-PILC
CEC (méq/100g)	72.93	24	21.33	17.33	13.33

Table 3: Cation exchange capacity (CEC) of the raw clay mineral and PILCs.

Component (%)	MF	MF01
Fe _(T)	59.76	64.12
SiO ₂	15.38	13.66
sCaO	4.87	6.29
K ₂ O	0.31	0.25
Na ₂ O	0.05	0.02
Al ₂ O ₃	5.03	3.90
MgO	0.77	0.69
SO ₃	0.01	0.24
P ₂ O ₅	0.12	0.15
TiO ₂	0.26	0.23
MnO	2.08	1.44
Cr ₂ O ₃	0.02	0.02
LOI	11.23	9.01

Table 4: Chemical composition and ignition loss (LOI) of the samples studied (MF and MF01) by XRF analysis.

Samples	S _{BET} (m ² /g)	S _{BJH/mesp} (m ² /g)	V _{BJH/mesp} (cm ³ /g)	V _{ads} (Cm ³ /g)	D(A°)
MF	44.393	35.173	0.096	0.11	19.073
MF01	45.868	44.170	0.092	0.10	18.989

S_{BET}: BET surface area, S_{mesp/BJH}: mesopore surface area, V_{mesp/BJH}: mesopore volume, V_{ads}: volume of N₂ adsorbed at P/P₀=0.98, D: average pore diameter.

Table 5: Textural properties of the studied samples: MF and MF01.

ores and the obtained patterns were shown on Figure 11. It can be explicitly considered that the same diffraction peaks have appeared in the XRD spectra of the two samples. Some diffractions are related to the presence of goethite FeOOH (2θ=21.2°, 34.96°, 36.8°, 41.4°, 50.5°, 53.2° and 59.3°) [49,50], hematite Fe₂O₃ (2θ=33.22°, 40.5° and 68.3°) [51] and magnetite Fe₃O₄ (2θ=35.5° and 61.3°) [52] iron phases. On the other hand, typical peaks of quartz (Q) and kaolinite (K) phases are detected. It should be noted that the XRD pattern of MF shows the same peaks which are less intense.

FT-IR analysis

In order to identify the functional groups of MF and MF01, FT-IR analysis was performed (Figure 12). Various functional groups represented in the IR spectra were the same as that of goethite. For MF, the absorption bands at about 894 and 797 cm⁻¹ are attributed to O-H bending bands in goethite (Fe-OH) and are respectively on behalf of the vibrations in and out of the plane [53]. The peaks at about 476.84; 538.27 and 600 cm⁻¹ are assigned to the symmetric stretching vibration bands of Si-O/Al-O and O-Fe-O functional groups, respectively [53,54]. The two bands around 538.27 and 476.84 cm⁻¹ can be attributed to hematite characteristic bands. The bands at 1046.09 cm⁻¹ and 1656 cm⁻¹ are related with asymmetric stretching vibration of Fe-O-Si, O-H respectively. Finally, the band between 3000 and 3400 cm⁻¹ corresponds to the hydrogen-bonded hydroxyl groups stretching vibration [53].

The FT-IR spectrum of MF01 shows that the chemical groups of MF01 are similar to the ones in MF sample. However, in MF01, the presence of C=O species is indicated by the band at 1451 cm⁻¹ correspond to asymmetric stretching vibration.

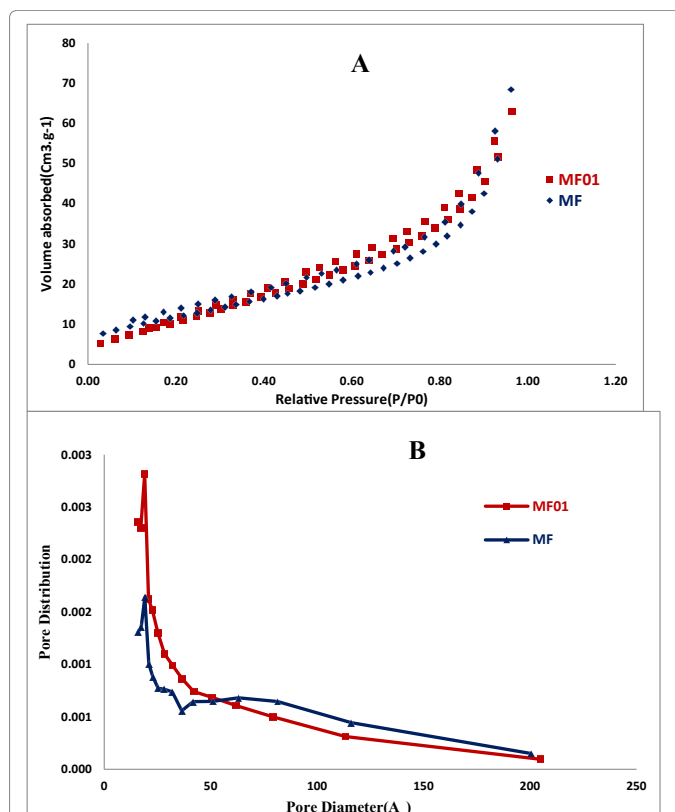


Figure 10: Nitrogen adsorption/desorption isotherms at 77K for iron-ores samples (A) and BJH-method pore size distribution curves from nitrogen sorption data (B).

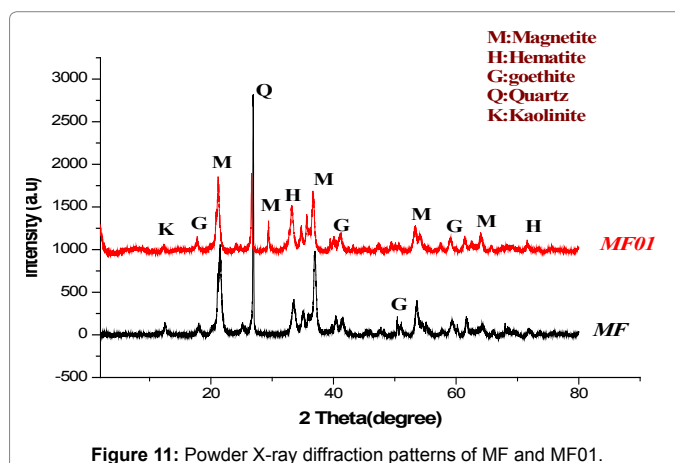


Figure 11: Powder X-ray diffraction patterns of MF and MF01.

Conclusion

In this work, clay with many properties was obtained through a simple, inexpensive and innovative route. The developed material is pillared smectite with mixed Al-Fe pillars between the clay layers. A care has been given to the physical and chemical properties of these catalysts. XR diffraction showed an increase in the basal spacing up to 19 Å. They have a high thermal stability. Textural characterization show a decrease in BET surface area indicating that a portion of the iron inserted into the clay structure is deposited on the surface, interacting with the tetrahedral sheets of the clay, without destroying the original framework. That change in the amount of iron on the surface of the

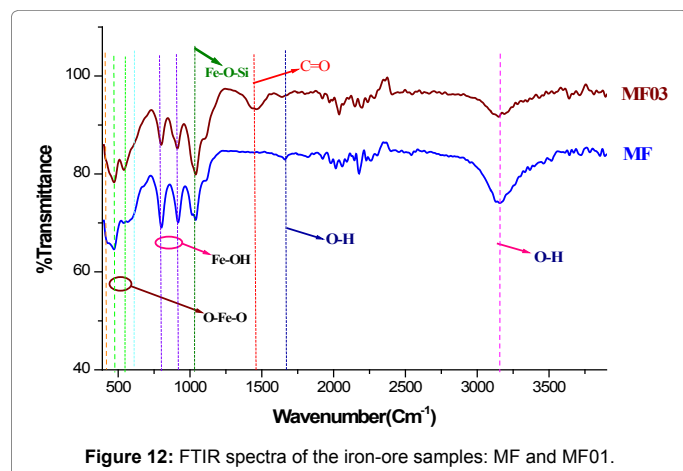


Figure 12: FTIR spectra of the iron-ore samples: MF and MF03.

material leads to a substantial increase in the adsorption and catalysis activity due to changes in the structure of surface sites available for the reaction to take place.

In addition, a natural catalyst was defined and characterized in this work: the iron-ore which is not a toxic compound and causes no secondary pollution in the environment. Regarding their physical and chemical properties, natural iron-ore will be utilized as a heterogeneous catalyst in the Fenton process.

Acknowledgements

The authors express their gratitude to the laboratory of Catalysis and Organic Synthesis of the University of Tlemcen, Algeria, for BET characterizations. They also are very grateful to the production laboratory in Bizerta cements CB especially the responsible Houcine TISS.

References

- Carriazo J, Guélou E, Barrault J, Tatibouet JM, Molina R, et al. (2005) Catalytic Wet peroxide oxidation of phenol by pillared clays containing AL-Ce-Fe. J Water Research 39: 3891-3899.
- Hadjitaief HB, DaCosta P, Beaunier P, Gálvez ME, Zina MB (2014) Fe-clay-plate as a heterogeneous catalyst in photo-Fenton oxidation of phenol as probe molecule for water treatment: Applied Clay Science 91: 46-54.
- Nogueira FGE, Lopes JH, Silva AC, Gonçalves M, Anastácio AS, et al. (2009) Reactive adsorption of methylene blue on montmorillonite via an ESIMS study. Appl Clay Sci 43: 190-195.
- Ramirez JH, Costa CA, Madeira LM, Mata G, Vicente MA, et al. (2007) Fenton-like oxidation of Orange II solutions using heterogeneous catalysts based on saponite clay. Appl Catal B: Environ 71: 44-56.
- Sum OSN, Feng J, Hu X, Yue PL (2004) Pillared laponite clay-based Fe nanocomposites as heterogeneous catalysts for photo-Fenton degradation of acid black 1. Chem Eng Sci 59: 5269-5275.
- Luna FJ, Schuchardt U (1999) Argilas pilarizadas-uma introdução: Quim. Nova 22: 104.
- Elizabeth G, Ramirez G, Sivaiah VM, Barrault J, Valange S, et al. (2012) Catalytic wet peroxide oxidation of phenol over iron or copper oxide-supported allophane clay materials: Influence of catalyst SiO₂/Al₂O₃ ratio. Microporous and Mesoporous Materials 162: 189-198.
- Corma A, Nemeth LT, Renz M, Valencia S (2001) Sn-zeolite beta as a heterogeneous chemoselective catalyst for Baeyer-Villiger oxidations. Nature 412: 423-425.
- Corma A, Iborra S, Mifsud M, Renz M, Susarte M (2004) A new environmentally benign catalytic process for the asymmetric synthesis of lactones: Synthesis of the flavouring d-decalactone molecule. Advanced Synthesis & Catalysis 346: 257-262.
- Renz M, Blasco T, Corma A, Fornes V, Jensen R, et al. (2002) Selective and shape-selective Baeyer-Villiger oxidations of aromatic aldehydes and cyclic

ketones with Sn-beta zeolites and H₂O₂. Chemistry-A European Journal 8: 4708-4717.

- Boronat M, Concepcion P, Corma A, Renz M, Valencia S (2005) Determination of the catalytically active oxidation Lewis acid sites in Sn-beta zeolites, and their optimisation by the combination of theoretical and experimental studies. Journal of Catalysis 234: 111-118.
- Barrault J, Bouchoule C, Echachoui K, Frini-Srasra N, Trabelsi M, et al. (1998) Catalytic wet peroxide oxidation (CWPO) of phenol over mixed (Al-Cu)-pillared clays. Applied Catalysis B: Environmental 15: 269-274.
- Barrault J, Abdellaoui M, Bouchoule C, Majeste A, Tatibouet JM, et al. (2000) Catalytic wet peroxide oxidation over mixed (Al-Fe) pillared clays. Applied Catalysis B: Environmental 27: L225-L230.
- Frini N, Crespin M, Trabelsi M, Messad D, Van Damme H, et al. (1997) Preliminary results on the properties of pillared clays by mixed Al-Cu solutions. Applied Clay Science 12: 281-292.
- Najjar W, Azabou S, Sayadi S, Ghorbel A (2007) Catalytic wet peroxide photo-oxidation of phenolic olive oil mill wastewater contaminants. Part I: reactivity of tyrosol over (Al-Fe) PILC. Applied Catalysis B: Environmental 74: 11-18.
- Ben Achma R, Ghorbel A, Dafinov A, Medina F (2008) Copper-supported pillared clay catalysts for the wet hydrogen peroxide catalytic oxidation of model pollutant tyrosol. Applied Catalysis A: General 349: 20-28.
- Tomul F, Balci S (2009) Characterization of Al, Cr-pillared clays and CO oxidation. Applied Clay Science 43: 13-20.
- Xiaofei X (2009) Fenton like oxidation of organic pollutants in the presence of iron (II,III) oxides. PhD Thesis, Nancy University, France and Wuhan University, China.
- Carriazo JG, Centeno MA, Odriozola JA, Moreno S, Molina R (2007) Effect of Fe and Ce on Al-pillared bentonite and their performance in catalytic oxidation reactions. Applied Catalysis A: General 317: 120-128.
- Valkaj KM, Kaselja I, Smolkovića J, Narendra Kumar SZ, Murzin DY (2015) Catalytic Wet Peroxide Oxidation of Olive Oil Mill Wastewater over Zeolite Based Catalyst. Chemical engineering transactions 43: 2283.
- Kasiri MB, Aleboye H, Aleboye A (2008) Degradation of acide blue 74 using Fe-ZSM5 zeolite as a heterogenous photo-Fenton catalyst. Appl Catal B: Environ 84: 9-15.
- Pariante MI, Martínez F, Melero JA, Botas JA, Velegraki TH, et al. (2008) Heterogeneous photo-Fenton oxidation of benzoic acid in water: Effect of operatin conditions, reaction by-products and coupling with biological treatment biological treatment. Applied Catalysis B: Environmental 85: 24-32.
- Cheknane B, Baudu M, Basly JPO, Bouras O (2010) Adsorption of basic dyes in single and mixture systems on granular inorganic-organic pillared clays. J Environmental Technology 31: 815-822.
- Tatibouët JM, Guélou E, Fournier J (2005) Catalytic oxidation of phenol by hydrogen peroxide over a pillared clay containing iron. Active species and pH effect. Top Catal 33: 225-232.
- Sapag K, Rojas S, Granados ML, Fierro JLG, Mendioroz S (2001) CO hydrogenation with Co catalysis supported on porous media. J Mol Catal A 167: 81-89.
- Francisco GE, Nogueira João HL, Adilson CS, Rochel ML, Jose DF, et al. (2011) Catalysts based on clay and iron oxide for oxidation of toluene. Applied Clay Science 51: 385-389.
- Ayari F, Srasra E, Trabelsi-Ayadi M (2005) Characterization of bentonitic clays and their use as adsorbent. Desalination 185: 391-397.
- Bankovic P, Milutinovic-Nikolic A, Jovic-Jovicic N, Dostanic J, Cupic Z, et al. (2009) Synthesis, Characterization and Application of Al, Fe-Pillared Clays. Acta Physica polonica, p: 115.
- Yuan P, Annabi-Bergaya F, Tao Q, Fan M, Liu Z, et al. (2008) A combined study by XRD, FTIR, TG and HRTEM on the structure of delaminated Fe-intercalated/pillared clay. J Colloid Interface Sci 324: 142.
- Mantin I (1969) Mesure de la capacité d'échange cationique des minéraux argileux par l'éthylène diamine et les ions complexes de l'éthylène diamine. CR Sci Paris 269: 815-818.
- Bergaya F, Vayer M (1997) CEC of clay, Measurement by adsorption of a copper éthylène diamine complexes. Appl Clay Sci 12: 275-280.

32. Jara A, Goldberg S, Mora ML (2005) Studies of the surface charge of amorphous aluminosilicates using surface complexation models. *J Colloid Interf Sci* 292: 160-170.
33. Bradley SM, Kydd RA (1993) Ga13, Al13, GaAl12, and chromium-pillared montmorillonites acidity and reactivity for cumene conversion. *Journal of Catalysis* 141: 239-249.
34. Cristofara AD, Violante A (2001) Effect of hydroxylaluminium species on the sorption and interlayering of albumin onto montmorillonite. *Applied Clay Science* 19: 59-67.
35. Caudo S, Centi G, Genovese CSP (2007) Copper-and iron-pillared clay catalysts for the WHPCO of model and real wastewater streams from olive oil milling production. *Applied Catalysis B: Environmental* 70: 437-446.
36. Letaef S, Blanca Casal PA, Martin-Luengo MA, Ruiz-Hitzky E (2003) Fe-containing pillared clays as catalysts for phenol hydroxylation. *Applied Clay Science* 22: 263-277.
37. Luo ML, Bowden D, Brimblecombe P (2009) Catalytic property of Fe-Al pillared clay for Fenton oxidation of phenol by H₂O₂. *Applied Catalysis B: Environmental* 85: 201-206.
38. Undabeytia T, Galán-Jiménez MC, Gómez-Pantoja E, Vázquez J, Casal B, et al. (2013) Fe-pillared clay mineral-based formulations of imazaquin for reduced leaching in soil. *Applied Clay Science* 80: 382-389.
39. Mandalia T, Crespin D, Messad D, Bergaya F (1998) Large interlayer repeat distances observed for montmorillonites treated by mixed Al-Fe and Fe pillaring solutions. *Chemical Communications* 19: 2111-2112.
40. Bergaya F, Aouad A, Mandalia T (2006) Pillared clays and clay minerals. In: Bergaya F, Theng BKG, Lagaly G (eds.), *Handbook of Clay Science*, pp: 393-421.
41. Bandosz TJ, Cheng K (1997) Changes in acidity of Fe-pillared/delaminated smectites on heat treatment. *Journal of Colloid and Interface Science* 191: 456-463.
42. Cañizares P, Valverde JL, SunKou MR, Molina CB (1999) Synthesis and characterization of PILCs with single and mixed oxide pillars prepared from two different bentonites. A comparative study. *Microporous and Mesoporous Materials* 29: 267-281.
43. Heylen I, Vansant EF (1997) The difference in adsorption capacity between Fe-PILCs and modified Fe-BuA- and Fe-Zr-PILCs. *Microporous Materials* 10: 41-50.
44. Reddy KM, Punnose A (2007) Occurrence and stability of ferromagnetism in chemically synthesized cobalt doped TiO₂. *J Mater Sci: Mater Electron* 18: 1137-1142.
45. Barrett EP, Joyner LG, Halenda PH (1951) Determination of pore volumes and area distributions in porous substances. I. Computation from nitrogen isotherms. *J Am Chem Soc* 73: 373-380.
46. Chmielarz L, Kustrowski P, Dziembaj R, Cool P, Vansant EF (2007) Selective catalytic reduction of NO with ammonia over porous clay heterostructures modified with copper and iron species. *Catalysis Today* 119: 181-186.
47. Fejes P, Kiricsi I, Kovacs K, Lazar K, Marsi I, et al. (2002) Incorporation of iron in sodalite structures and their transformation into other iron containing zeolites-synthesis of Fe-NaA (LTA). *Applied Catalysis A: General* 223: 147-160.
48. Jaiswal A, Banerjee S, Mani R, Chattopadhyaya MC (2013) Synthesis, characterization and application of goethite mineral as an adsorbent. *J Environ Chem Eng* 1: 281.
49. Markovski JS, Dokic V, Milosavljevic M, Mitric M (2014) Ultrasonic assisted arsenate adsorption on solvothermally synthesized calcite modified by goethite, α-MnO₂ and goethite/α-MnO₂. *Ultrason Sonochem* 21: 790-801.
50. Tireli AA, Guimarães IR, Terra JCS, da Silva RR, Guerreiro MC (2015) Fenton-like processes and adsorption using iron oxide-pillared clay with magnetic properties for organic compound mitigation. *Environ Sci Pollut Res* 22: 870-881.
51. Schwertmann U, Cornell RM (2008) *Iron Oxides in the Laboratory. Preparation and Characterization*. Wiley-VCH, New York, USA.
52. Oliveira LCA, Ramalho TC, Souza EF, Gonçalves M, Oliveira MC, et al. (2008) Catalytic properties of goethite prepared in the presence of Nb on oxidation reactions in water. Computational and experimental studies. *Appl Catal B: Environ* 83: 169-176.
53. Sankaramakrishnan N, Gupta A, Viduarthi SB (2014) Enhanced arsenic removal at neutral pH using functionalized multiwalled carbon nanotubes. *J Environ Eng* 2: 802.
54. Cai J, Chen S, Ji M, Hu J, Ma Y, et al. (2014) Organic additive-free synthesis of mesocrystalline hematite nanoplates via two dimensional oriented attachment. *Cryst Eng Comm* 16: 1553-1559.